



Recent advances in automated imaging have enabled high-content quantification of tumor phenotypes to aid cancer drug discovery.

High-content multiplexed tissue imaging and quantification for cancer drug discovery

Beverly L. Falcon^{1,6}, Julie Stewart^{2,6}, Scharri Ezell¹, Jeff Hanson³, John Wijsman², Xiang Ye⁴, Eric Westin⁴, Greg Donoho², Kelly Credille⁵ and Mark T. Uhlik¹

¹ Eli Lilly and Company, Department of Cancer Angiogenesis, Lilly Corporate Center, Indianapolis, IN 46285, USA

² Eli Lilly and Company, Department of Translational Science, Lilly Corporate Center, Indianapolis, IN 46285, USA

³ Eli Lilly and Company, Department of IT, Lilly Corporate Center, Indianapolis, IN 46285, USA

⁴ Eli Lilly and Company, Department of Oncology, Lilly Corporate Center, Indianapolis, IN 46285, USA

⁵ Eli Lilly and Company, Department of Investigational Pathology, Lilly Corporate Center, Indianapolis, IN 46285, USA

Targeting multiple hallmarks of cancer with drug combinations may provide unique opportunities for cancer therapeutics; however, phenotypic quantification is necessary to understand *in vivo* mechanisms of action of each drug alone or in combination. Immunohistochemistry (IHC) can quantify phenotypic changes, but traditional methods are not amenable for high-throughput drug discovery. In this article, we describe a high-content method to quantify changes in tumor angiogenesis, vascular normalization, hypoxia, tumor cell proliferation, and apoptosis using IHC. This method to quantify tumor model phenotypes can be useful for cancer drug discovery by increasing the understanding of: (i) tumor models used in efficacy studies, (ii) changes occurring during the growth of the tumor, and (iii) novel mechanisms of actions of cancer therapeutics.

Introduction

The hallmarks of cancer describe the underlying principles and complexity of most tumors [1,2]. They include sustained proliferative signaling, evasion of growth suppressors, resistance to cell death, replicative immortality, genomic instability and mutation, angiogenesis, invasion and metastasis, reprogrammed energy metabolism, tumor promoting inflammation and evasion of immune destruction [1,2]. Drugs that interfere with each of these fundamental traits of cancer cells have been developed. However, cancer cells may reduce their dependence on a particular phenotype and become more dependent on another in response to therapy [1,2]. For example, studies indicate that vascular endothelial growth factor (VEGF) inhibitors potentially inhibit angiogenesis and can lead to reductions in short-term tumor growth. However, preclinical studies have shown that continued VEGF suppression leads to an adaptation of the tumor cells

Corresponding author: Uhlik, M.T. (uhlik_mark_t@lilly.com)

⁶ BLF and JS contributed equally to this work.

Dr Beverly L. Falcon is currently a postdoctoral scientist at Eli Lilly and Company. She specialized in the characterization of novel cancer therapeutics by immunohistochemistry in collaboration with multiple companies as a postdoctoral fellow in the laboratory of Dr Donald McDonald at the University of California, San Francisco. In 2011, she joined Eli Lilly to expand upon her expertise and develop high-throughput methods to quantify sections stained by immunohistochemistry. Her interests are in the development and characterization of multiplexed immunohistochemical panels to understand unique mechanisms of actions of drugs on tumor biology, development of high-throughput cell-based assays, and identification and characterization of novel antiangiogenic targets for cancer therapy.



Julie Stewart is currently a consultant biologist in the Molecular Pathology and Imaging Lab in the Translational Sciences and Technologies department at Eli Lilly. She received her B.S. in Zoology at SIU-Carbondale and her M.S. in Veterinary Pathobiology at the University of Illinois after which she worked in the Department of Animal Sciences at UI and at Searle/Pharmacia in St. Louis. Since moving to Eli Lilly, Julie has worked as a discovery biologist for projects in inflammation and oncology. Most recently, she has applied her expertise in high-content imaging to analyze phenotypic changes in tumors caused by modulation of various oncology targets.



Dr Mark Uhlik is currently a principal research scientist in Oncology Discovery Research at Eli Lilly and Company. Mark received his Ph.D. in Microbiology and Immunology from the Pennsylvania State University College of Medicine. After completing postdoctoral training fellowships at University of Colorado Health Sciences Center and University of North Carolina College of Medicine, Dr Uhlik joined Eli Lilly in the Fall of 2004. As a research scientist with Lilly he has served as the Lead Biologist for several Oncology drug discovery projects, including the Angiogenesis Phenotypic Drug Discovery Project, and made significant scientific contributions to several others. Dr Uhlik is also leading multiple efforts in the development and implementation of high-content cellular imaging assays and quantitative, multiplexed analysis of tissues. His expertise in imaging technologies and phenotypic drug discovery has resulted in numerous productive collaborations with scientists across the pharmaceutical industry and academia.



to be less dependent on angiogenesis and instead promotes tumor invasion and metastasis [3,4]. Adaptive shifts in these capabilities may limit the efficacy of analogous hallmark-targeting therapies and suggests that drug development and treatment protocols could benefit by targeting multiple functionally discrete tumor characteristics. One challenge faced when developing these combinations, however, is phenotypic quantification of *in vivo* mechanisms of action on multiple hallmarks of cancer. Multiplexed immunohistochemical assays in which various cellular parameters and tissue phenotypes are measured may offer a unique approach towards this end.

Immunohistochemistry (IHC) is a powerful and widely used diagnostic tool. It detects protein expression levels similar to Western blotting and ELISA. Unlike these traditional methods, which use a homogeneous tumor extract, IHC allows for the detection of spatial protein expression patterns. This is particularly advantageous when assessing the effects of novel drugs targeting tumor cells, stromal cells, or both in a heterogeneous tumor. This maintenance of spatial relationships prevents signal dilution that is observed if 100% of the cells do not express the signal. Thus, unlike Western blotting and ELISAs, IHC has the ability to detect both the intensity of the signal and the percentage of cells expressing that protein. Finally, the capability to perform IHC on small tissue biopsies and the ability to archive tissues in paraffin for long-term storage also make IHC highly amenable for drug discovery efforts.

IHC has been widely used for preclinical studies to characterize mechanisms of actions for cancer therapeutics targeting the tumor cells or the tumor blood vessels. Thus, there are many readily available antibodies that have been developed and validated for the detection of blood vessels, pericytes, basement membrane, proliferation, apoptosis and hypoxia. IHC studies are becoming more routinely used to show changes in tumor vessel number, density and morphology in addition to the relationships of these vascular changes to effects on tumor cell hypoxia, proliferation and/or apoptosis [5–16]. These studies have been instrumental in understanding the mechanisms of action of chemotherapeutics [6,7,10,11] and novel drugs such as inhibitors of Delta-like ligand 4 [12,13], VEGF [5,8,9,16], Angiopoietin 2 (Ang2) [8] and platelet-derived growth factor (PDGF) [5,7,14,15]. However, the conventional approaches for quantifying these parameters are time-consuming and involve either area density measurements or semi-quantitative hand counts and scoring by pathologists on ‘representative’ fields of the heterogeneous tumor. Thus, the traditional use of IHC has not been amenable for high-throughput drug discovery.

Over the past decade, many multiplexed high-content cellular assays based on fluorescent imaging have been developed to measure multiple cellular parameters and define relationships between molecular target activities, subcellular localization and morphologic features. Although the use of high-content analysis has flourished in the *in vitro*, cell-based arena, few laboratories have adopted similar methods to support *in vivo* studies.

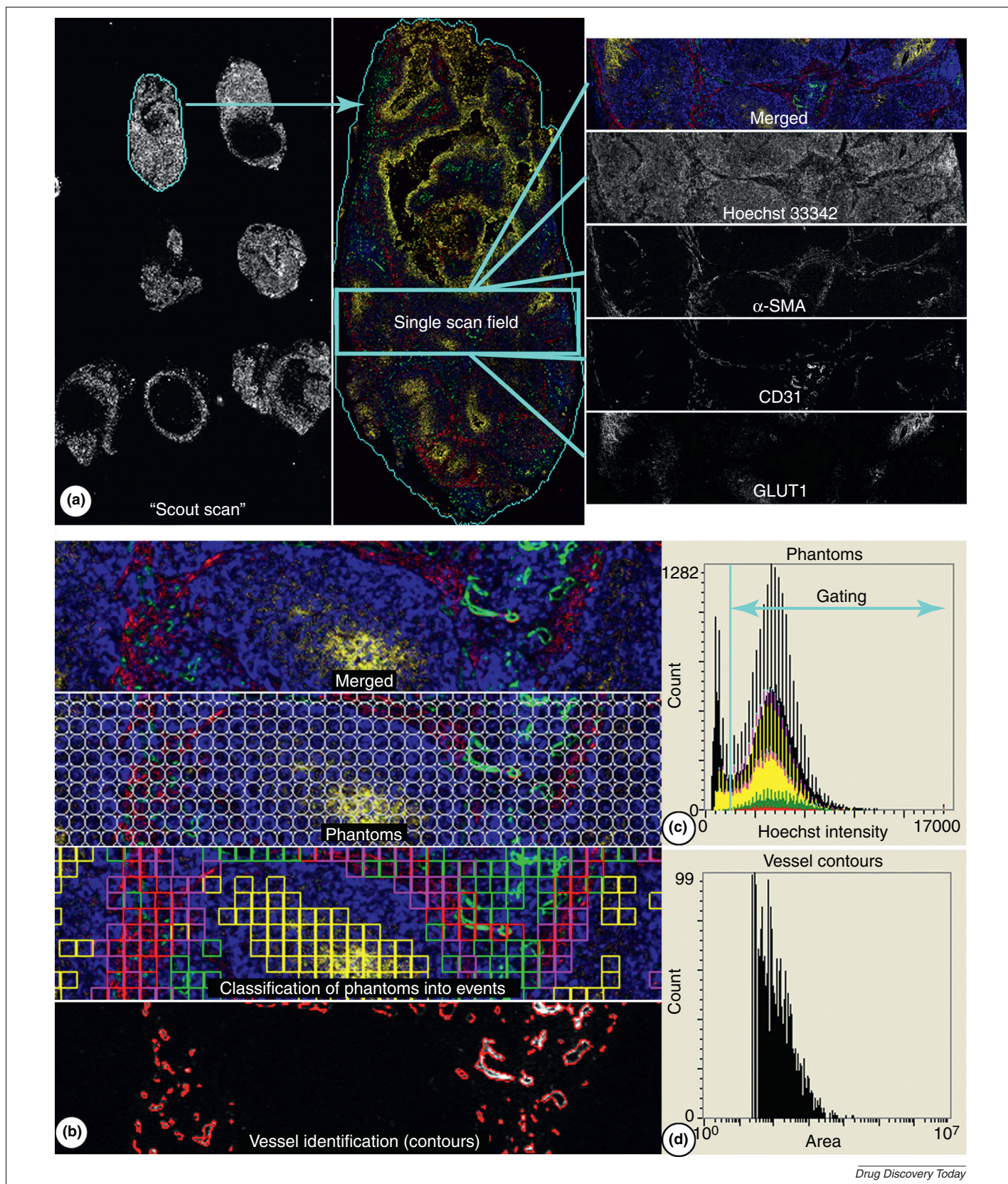
In this article, we describe a high-content method to effectively and efficiently quantify effects of novel cancer therapeutics on tumor angiogenesis, vascular normalization, hypoxia, proliferation and apoptosis on tissue sections from *in vivo* studies. The method is high throughput and the quantifications are based upon the entire tumor section rather than on random or ‘representative’

fields. We also describe how this method is useful for cancer drug discovery by increasing the understanding of: (i) differences between xenograft models for *in vivo* model selection, (ii) the phenotypic characterization of xenograft growth and (iii) mechanisms of action of novel drugs.

Development of multiplexed, fluorescence-based IHC panels

As our understanding of the complexity of cancer increases, it is becoming evident that the assessment of *in vivo* mechanisms of action on multiple hallmarks of cancer is necessary for drug discovery. These measurements not only evaluate the effectiveness of a particular drug, but may also lead to the development of novel drug combinations. To support these aims, we developed fluorescence-based multiplexed IHC panels that identify general phenotypic hallmarks of cancer applicable to most tumor models used in cancer drug discovery (Supplemental Table 1 and Supplemental Methods). This approach allows the identification of multiple phenotypes in a single tissue section with a high degree of quantification and maintenance of cellular spatial relationships. These panels are used across many cancer drug discovery platforms and allow for comparisons across multiple studies.

For the ‘angiogenesis panel,’ tumor vessels or endothelial cells are stained with CD31, pericytes or mural cells with Alpha-Smooth Muscle Actin (SMA), and hypoxic regions with Glucose Transporter-1 (GLUT1) (Supplemental Figure 1A and Supplemental Methods). This panel allows for the assessment of the effects of drugs on angiogenesis and the regulation of cellular energetics. Angiogenesis, or the sprouting of new blood vessels from existing ones, is necessary to deliver nutrients and oxygen and evacuate metabolic waste and carbon dioxide. Tumors will not grow beyond 2–3 mm in diameter *in vitro* or approximately 1 mm in diameter *in vivo* without inducing new blood vessel growth [16,17]. Pericytes are a key component of the microvasculature contributing to blood vessel maturation and stabilization, normal endothelial cell function and blood flow regulation [18–20]. Inhibition of PDGF-B, a key growth factor for pericyte recruitment, leads to pericyte loss and eventually tumor vessel regression [14]. In addition, pericyte association with tumor vessels is used as an indication of vessel normalization [16,21]. Compared to normal vessels, tumor blood vessels have multiple structural and functional abnormalities (Supplemental Figure 1B) [22]. Vascular normalization, as evidenced by decreased tortuosity and increased pericyte coverage of tumor vessels after antiangiogenic therapy (Supplemental Figure 1B arrows), may increase tumor vessel function and improve the delivery of other cancer therapeutics [21,23]. Finally, tumor hypoxia occurs when tumor cells have been deprived of oxygen. Due to the functional abnormalities of the tumor vasculature, hypoxia is often found in tumors even if abundant vessels are detected. In addition, hypoxia is often induced following regression of vessels with antiangiogenic agents. Responses to hypoxia can lead to increases in some hallmark characteristics. For example, increased HIF-1 α expression in response to hypoxia can increase growth factor expression to induce angiogenesis or increase cMET expression to stimulate tumor cell invasion and metastasis [24,25]. GLUT1 is upregulated by HIF-1 α and can be used as a surrogate marker for hypoxia [26–28]. In many of our tumor models GLUT1 staining is found approximately 100 μ m from the tumor vessels (Supplemental Figure 1A). This is

**FIGURE 1**

iCys image capturing and analysis. **(a)** A 'scout scan' of the whole slide identifies tumors based on Hoechst staining (left). Each tumor is then scanned for the immunohistochemical markers. Shown is an example of a tumor stained with the angiogenesis panel (middle). The microscope takes individual scan fields and pieces them together to obtain the entire tumor. For the angiogenesis panel, each scan field has staining for Hoechst, SMA, CD31 and GLUT1 (right). **(b)** A single scan field demonstrates the sample grids that are used to identify and classify phantoms and an example of how the system identifies and classifies vessels based on contouring. **(c)** Each phantom is graphed based on its Hoechst intensity to gate for only phantoms with Hoechst positive staining. **(d)** Vessels identified by contouring are graphed based on the area of each contour.

consistent with previous studies showing that the distance between blood vessels and the most distant viable cells in tumors is dependent on oxygen and has a mean distance of 105 μm [29].

In the 'tumor health panel,' CD31 identifies blood vessels, TUNEL measures apoptosis, and Ki67 assesses proliferation (Supplemental Figure 1C and Supplemental Methods). This panel is designed to measure effects on angiogenesis, resistance to cell

death, sustained proliferative signaling, and evasion of growth suppressors. Tumor growth is dependent on both sustained proliferative signaling and inhibition of programmed cell death or apoptosis. Proliferative and apoptotic tumor regions are dependent on nutrient and oxygen delivery by the tumor vasculature as proliferating tumor cells are found adjacent to the tumor vessels whereas apoptotic cells are found a distance from the vessels, often

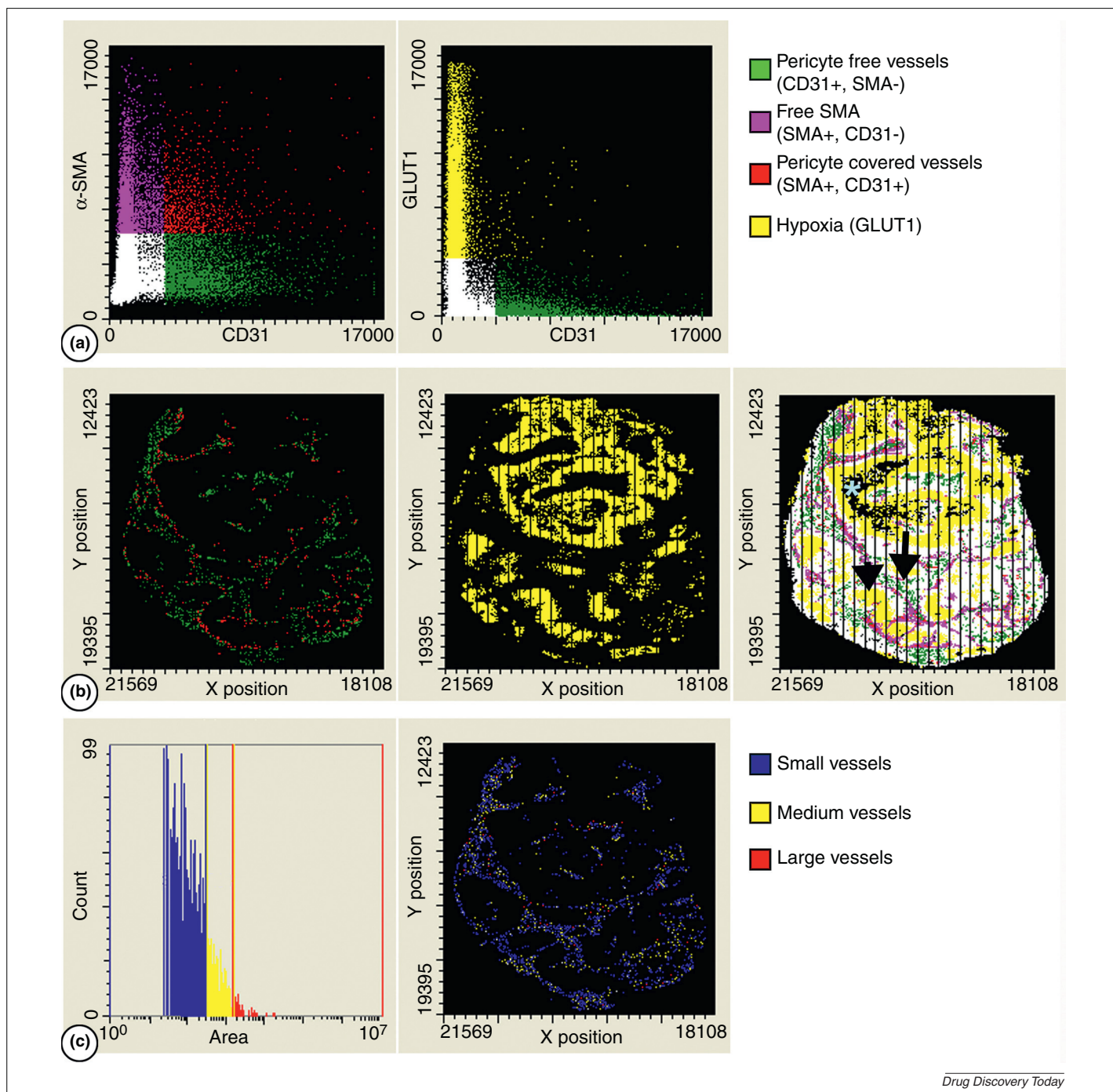


FIGURE 2

Angiogenesis panel readouts. **(a)** Phantoms are displayed on a scatterplot and gated for CD31 and SMA expression (left) or GLUT1 expression (right). On the basis of this gating, pericyte-free vessels (highlighted in green), free SMA (highlighted in magenta), pericyte-covered vessels (highlighted in red), and hypoxia (highlighted in yellow) are identified. **(b)** Expression maps show the phantoms identifying pericyte-free and pericyte-covered vessels (left), GLUT1 (middle), and all gates (right). Expression maps help identify associations between vascularized regions (arrow), hypoxic areas (arrowhead), and necrotic regions (blue asterisk). **(c)** Vessel sizes are shown as a histogram demonstrating the three different sizes of vessels based on the contoured area (left). Expression of a whole tumor showing small (blue), medium (yellow), and large (red) vessels based on contouring (right).

in regions of GLUT1 expression (Supplemental Figure 1A and C). To assess drug effects on the overall 'tumor health' and ability of tumors to grow, IHC of both proliferation and apoptosis is necessary. These multiplexed IHC panels, referred to herein as 'angiogenesis' and 'tumor health' panels, represent the foundation for a methodology that can be broadly used across numerous tumor types and provide quantitative data to drive key decisions for multiple drug discovery efforts.

Automated, high-content data acquisition of IHC panels

Traditionally, IHC has been impractical to use for drug discovery efforts because the imaging and quantifications are labor intense and time-consuming. Quantifications are typically made on five to ten 'representative' fields of the whole tumor and are dependent on either separate image analysis software or needs to be read by a trained pathologist. Because tumors are very heterogeneous, it is possible that representative regions are biased and do not reflect the biological processes occurring across the entire tumor [30]. However, image collection and analysis for an entire tumor cross-section is often slow and impractical. For our studies, an iCys research imaging cytometer is used to automatically capture and analyze the data in a high-throughput manner. The automated stage allows for scanning of one to nine whole tumor cross-sections per slide (Fig. 1a). Slide carrier units hold up to four slides and robotics can be used to automatically load and unload slide carrier units. Image acquisition using the iCys is very quick. After an approximately 20 min scout scan of all the tumors and slides in a carrier unit, the acquisition and analysis of each tumor takes approximately 2.5 min. Analyses of the studies are unbiased, as quantifications are based on

a whole tumor cross-section and the same algorithms are used to equivalently process the data across different tumors and treatment groups. In addition, the digital nature of the images easily allows for reprocessing and reanalysis using new algorithms. Thus, this set-up can easily and automatically evaluate the effects of multiple drugs at multiple concentrations and various time points with minimal human intervention or error.

To acquire the images, the iCys first performs a 'scout' scan. Using one fluorophore, such as a nuclear stain like Hoechst 33342, the machine scans the entire slide and identifies tumors by contouring each tumor cross-section as an individual object or region of interest (ROI). In the next process, individual scan fields of the tumor cross-section are taken for each fluorescent channel. The individual scan fields are automatically stitched together to give an image of the entire tumor cross-section (Fig. 1a). Quantifications are made on each of these whole cross-sectional tumor images. A stereology-based analysis by means of a grid of sampling elements called phantoms is used to classify and color code individual events based on the characteristic fluorescence (Fig. 1b). Phantoms assess and quantify fluorescence expression of the image independent of individual pixel or 'object' events. This allows for high computation speed, quick analysis of the entire heterogeneous tumor, and less human bias. The size of the phantoms can be adjusted, but smaller phantoms require more time, computing power, and memory for analysis. Random patterns of phantoms can also be used, but may be inaccurate and limit the ability to relate multiple events to one another. Thus, a balance must be reached in which the phantoms are small enough and close enough to capture the changes in events, but large enough to

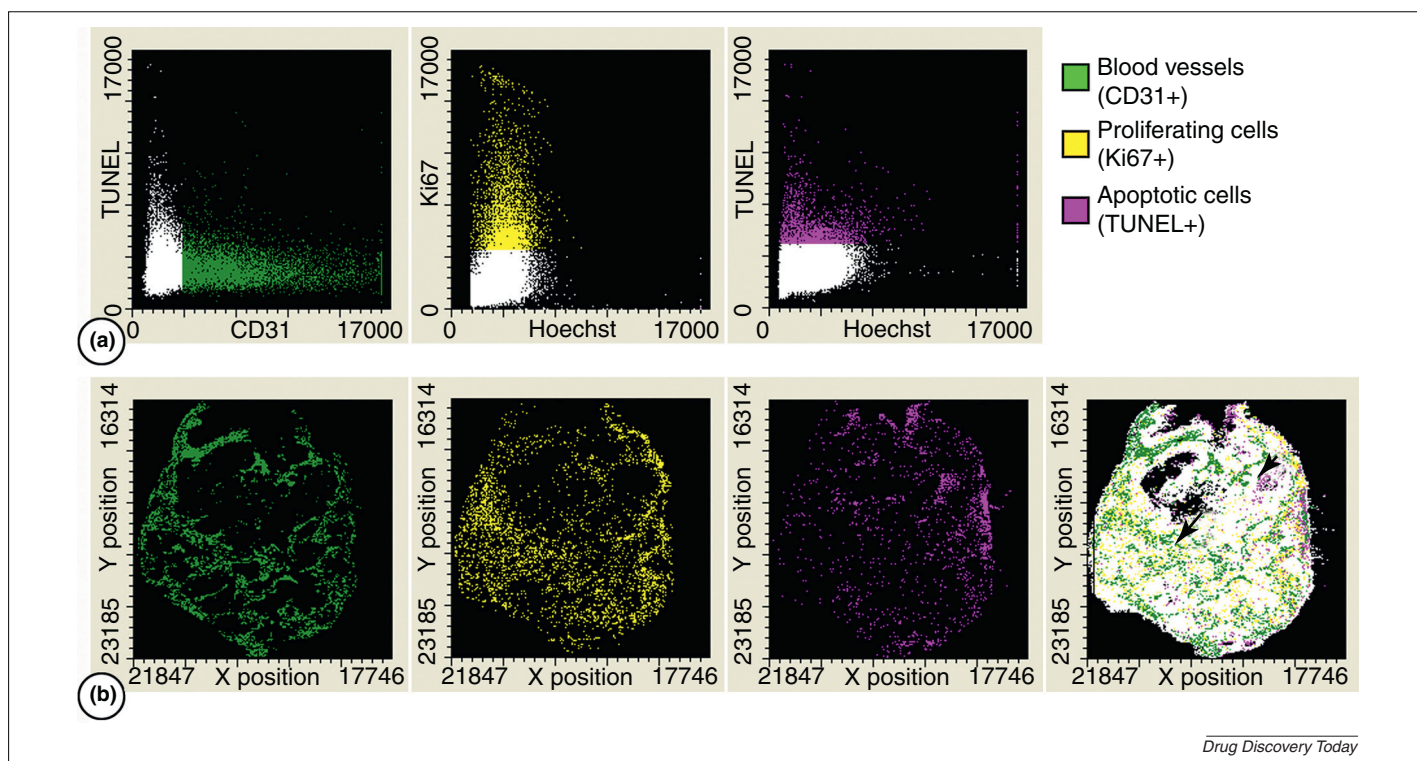


FIGURE 3

Tumor health panel readouts. (a) Scattergrams illustrating the gating used to identify positive staining for CD31 (green), Ki67 (yellow), and TUNEL (magenta). (b) Expression maps of the whole tumor illustrating phantoms for CD31 (green), Ki67 (yellow), TUNEL (magenta), The merged expression map illustrates that vascularized regions are associated with proliferating areas (arrow), but not hypoxic regions (arrowhead).

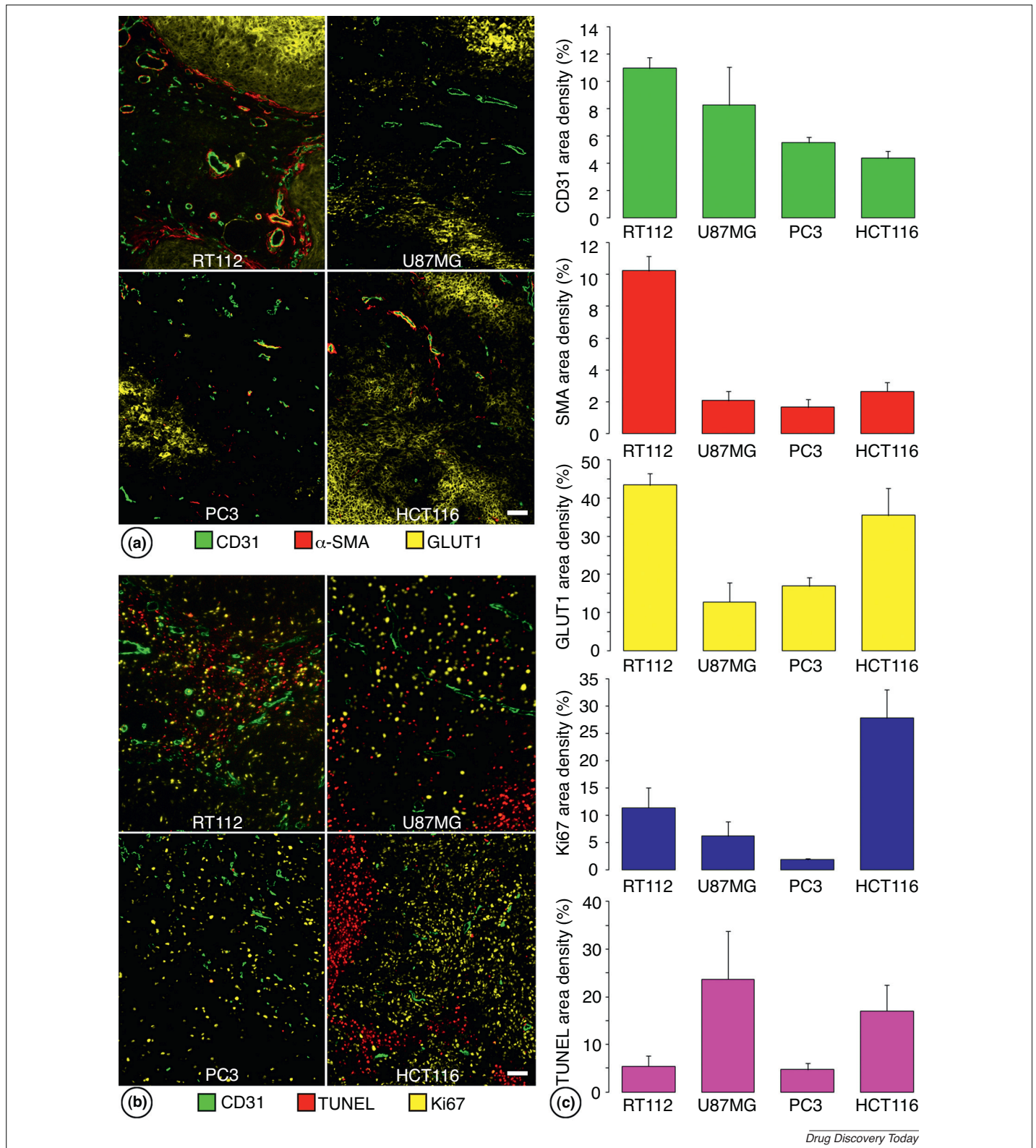
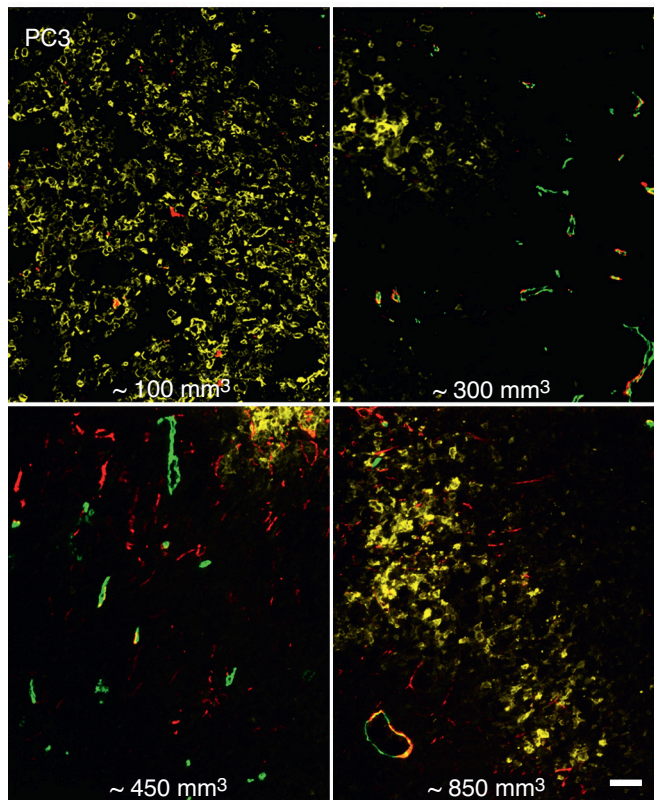
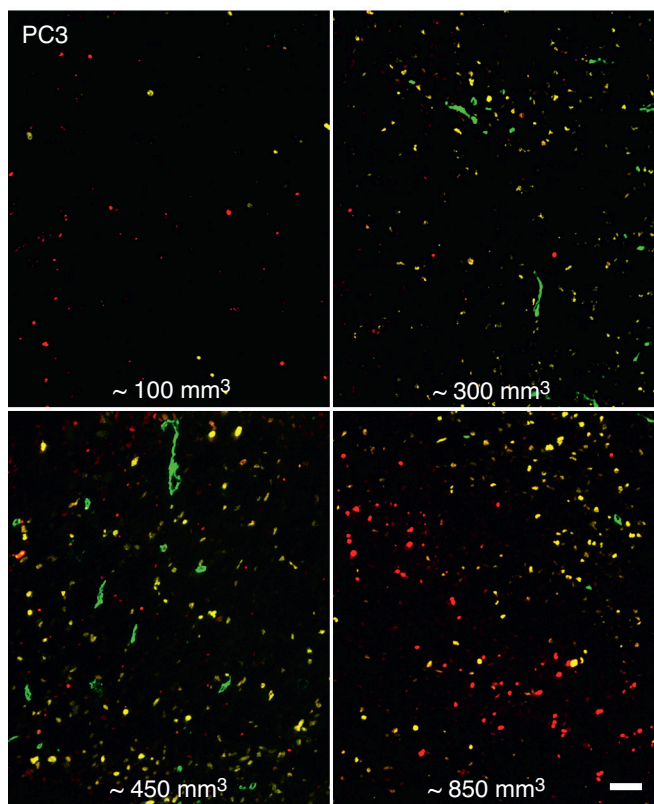


FIGURE 4

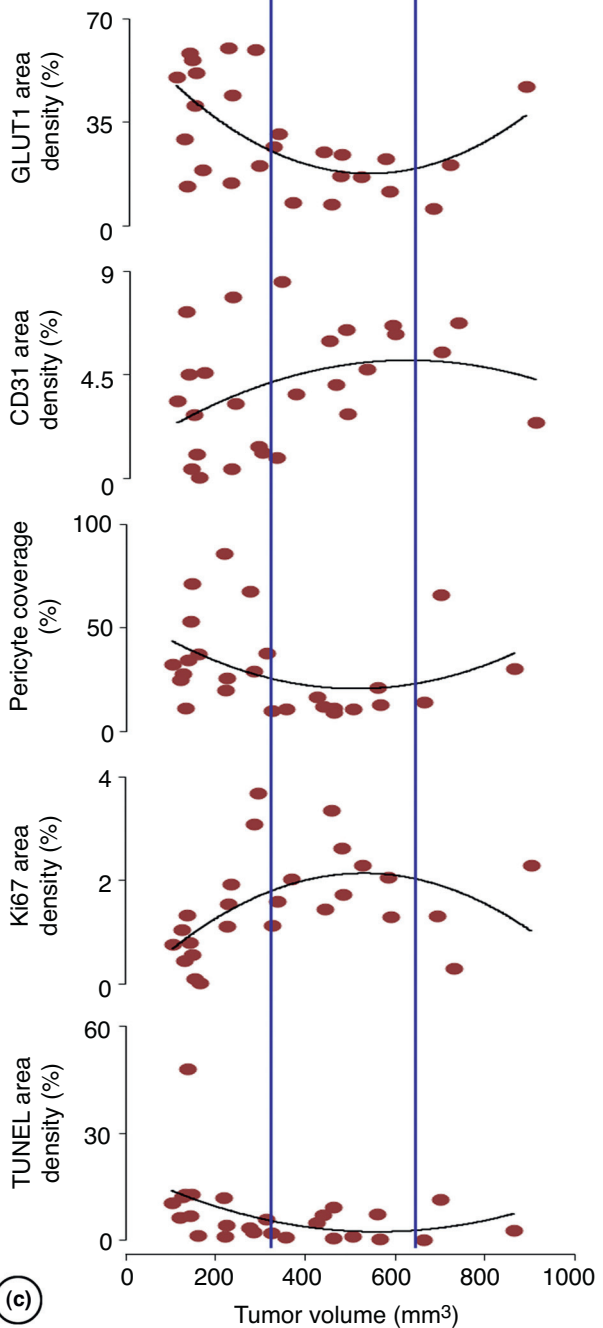
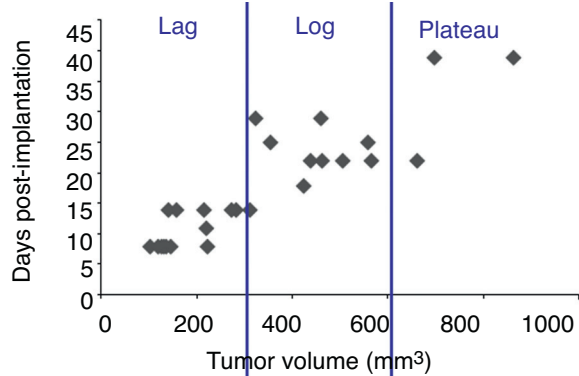
Comparison of tumor models. **(a)** Angiogenesis panel staining for blood vessels (CD31; green), SMA (red), and hypoxia (GLUT1; yellow) of four different xenograft models; RT112 (top, left), U87MG (top, right), PC3 (bottom, left), and HCT116 (bottom, right). **(b)** Tumor health panel staining for blood vessels (CD31; green), apoptotic cells (TUNEL; red), and proliferating cells (Ki67; yellow) of four tumor models. **(c)** Quantification of baseline area densities of CD31 (green), SMA (red), GLUT1 (yellow), Ki67 (blue), and TUNEL (magenta) in RT112, U87MG, PC3, and HCT116 tumor models. Scale bar is 50 μ m in (a) and (b).



(a) ■ CD31 ■ α-SMA ■ GLUT1



(b) ■ CD31 ■ TUNEL ■ Ki67



Drug Discovery Today

still allow analysis in a high-content manner. All phantoms are graphed based on Hoechst intensity allowing for gating to exclude non-tumor (Hoechst-negative) regions (Fig. 1c) from further analysis. Multicellular objects, such as tumor blood vessels, are also identified and quantified based on discrete contouring of each individual vessel (Fig. 1b). Object data is independently graphed as histograms of the area of each blood vessel (Fig. 1d). After the images of the tumor cross-sections are collected and the phantoms and contours are acquired, analysis of the data is largely based on flow cytometry-based algorithms as described below. Once the algorithms are established, this creates a high-throughput platform that is both versatile and easy to use.

Phenotypic assessment of the tumor vasculature using the angiogenesis panel

The angiogenesis panel comprises vessel, pericyte, and hypoxia markers to enable density, morphology, stability, and functional assessment of the vasculature. Similar to flow cytometry, phantoms are graphed based on the intensities of several fluorophores in scatterplots and gated into populations and subpopulations. For the angiogenesis panel, CD31 and SMA intensities are plotted on a scattergram where individual gating identifies three populations: phantoms designating pericyte-free blood vessels (CD31 only), phantoms designating pericyte-covered blood vessels (CD31 and SMA), and phantoms designating myofibroblasts not associated with the blood vessels (SMA only; Fig. 2a). GLUT1 phantoms are graphed and gated for positive hypoxia staining (Fig. 2a). After acquisition of all fluorescent channels across the whole tumor, expression maps are created to visualize phenotypic associations between the different markers (Fig. 2b). For some tumor models, the angiogenesis panel shows a compartmentalization between the stromal regions containing CD31 and SMA staining (arrow) and hypoxic areas with GLUT1 staining (arrowhead; Fig. 2b). Even further from the blood vessels, necrotic (Hoechst-negative) cells are seen (asterisk). This compartmentalization indicates that there is a viable region near the stromal cells, but past a certain distance, the nutrients and oxygen availability are limited and hypoxia is seen. The width of this sleeve of viable tumor cells surrounding blood vessels has previously been used as an indicator of blood vessel function [7].

Contours of tumor blood vessels are used to generate additional indices, such as tortuosity and vessel normalization, to describe complex vascular phenotypes. The histogram of the blood vessel contour areas are gated into different sized vessels (small, medium and large) and an expression map of the different sizes of blood vessels are shown (Fig. 2c).

On the basis of the gating of the scatterplots, the number of phantoms of the various populations is given for each tumor (Supplemental Table 2). Mean and standard errors are calculated from all the tumors in a given group. From the phantom readouts,

more traditional measurements such as area densities for CD31, SMA, pericytes (defined as SMA positive staining associated with blood vessels) and GLUT1 are calculated as described in the methods (Supplemental Table 2). The amount of pericyte coverage is assessed by comparing the number of CD31, SMA phantoms to total CD31 positive phantoms (Supplemental Table 2).

From the object contouring of tumor blood vessels, the percentages of vessels that have small, medium or large areas are determined (Supplemental Table 2). Tortuosity and normalization indices are also calculated based on these contours. Tortuosity of tumor vessels has been described, but quantification of this phenomenon has traditionally been difficult [21,22]. For our quantifications, we compare the number of large and small vessels. This is based on the assumption that the tortuous tumor vessels are disorganized and run in multiple directions whereas less tortuous vessels or vessels found in normal tissues are more directionally aligned. The aligned vessels are typically cut in cross-section and are smaller in size. Tortuous tumor vessels, however, can be cut in cross-section, longitudinally, or at any angle in between. Thus, if a treatment causes the tumor vessels to be less tortuous, the vessels will be better aligned and this will be reflected when comparing the percent of large and small vessels. On the basis of our pericyte coverage, tortuosity index, area density of hypoxia, and blood vessel area density results, we calculate a vascular normalization index (Supplemental Table 2). This calculation assumes that if pericyte coverage increases and tortuosity and hypoxia decrease, then vascular normalization is increased.

Area density readouts are good indications of whether a particular drug has effects on the number of blood vessels or pericytes. Previous studies have shown significant reductions in CD31 area density with VEGF inhibitors [5,8,9,16,31] and pericyte area density with PDGF inhibitors [5,7,14,15], but these reductions are not always associated with reduced tumor growth [14]. In addition, blockade of the delta-like 4 – notch signaling pathway results in excessive tumor vessels with reduced tumor growth [32]. Together, these studies indicate that vessel function may be a better predictor of tumor efficacy than overall vessel number [7,12,13]. Therefore, more elaborate quantifications are necessary to understand the effects of drugs on tumor vessel function. To do this, our algorithms are designed to also calculate the area density of hypoxia, pericyte coverage, tortuosity and normalization of the tumor vessels. These calculations are performed automatically and do not require separate images or quantifications to be performed.

Determining the relationship between blood vessels and tumor cell proliferation and apoptosis with the tumor health panel

Although changes in the tumor vessels are important in studying the mechanisms of actions of certain drugs, we are ultimately

FIGURE 5

Characterization of tumor growth. Examination of the tumor growth characteristics by staining PC3 tumors at four different sizes (~100, 300, 450 and 850 mm³) with antibodies for the angiogenesis panel (a) and the tumor health panel (b). (c) Scatterplot of the tumor volume at different time periods (top) shows three phases of PC3 tumor growth; lag, log, and plateau. Scatterplots illustrate changes in GLUT1, CD31, Ki67 and TUNEL area densities and pericyte coverage of tumor vessels during each phase of PC3 tumor growth. Scale bar is 50 μm in (a) and (b).

concerned with whether or not a particular drug affects tumor growth. Therefore, relationships between the tumor vasculature and tumor cell proliferation and apoptosis are important. Thus, we have also developed a tumor health panel that examines tumor cell proliferation and apoptosis in relationship to tumor blood vessels. Scatterplots of the intensities of the fluorophores are gated to quantify the number of CD31, Ki67 or TUNEL positive phantoms (Fig. 3a). Expression maps of phantoms identifying the tumor health panel show tumor vessels associated with proliferating regions (arrow) and apoptotic cells in non-vascularized regions (arrowhead) (Fig. 3b). Similar to the angiogenesis panel, area densities of CD31, TUNEL and Ki67 are calculated from the gated phantoms (Supplemental Table 3). CD31 area density in both the angiogenesis and tumor health panels allows for control of section-to-section variability and quality control of the tissues. In this example, the area densities of CD31 are comparable in serial sections stained for the angiogenesis (10.24 ± 1.15) and tumor health (9.53 ± 0.95) panels (Supplemental Tables 2 and 3). Evaluation of multiple sections throughout the tumor indicates little variability from the first sections to the last sections of a tumor block when evaluating the whole tumor (data not shown). This is probably due to our quantifications being based on the whole tumor cross-section which allows us to capture the tumor heterogeneity in one section of the tumor. Together, the data obtained from the angiogenesis and tumor health panels provides a comprehensive view of the phenotype of a tumor.

Multiplexed tissue imaging for baseline profiling of multiple tumor models

One of the most important considerations in drug discovery is the selection and characterization of appropriate *in vivo* models. This is particularly challenging when selecting between very heterogeneous and diverse tumor models. Thus, having a systematic, high-throughput, and replicable approach that is comparable across tumor models can help drug discovery programs choose the right tumor models for the right targets.

To better understand the phenotypes of some commonly used xenograft models, four tumor models (RT112 – bladder; U87MG – glioblastoma; PC3 – prostate and HCT116 – colorectal) of roughly the same size (400–800 mm³) were profiled using the described angiogenesis and tumor health panels (Fig. 4). The RT112 model had the greatest amount of tumor blood vessels, SMA and hypoxia, but had less proliferation and apoptosis compared to the other models (Fig. 4). By contrast, the HCT116 model had few blood vessels and little SMA staining, but high levels of hypoxia, proliferation, and apoptosis (Fig. 4). Therefore, for studies targeting the cell cycle, a model such as HCT116 with high Ki67 may be the most sensitive model to use (Fig. 4). However, for drug discovery programs targeting angiogenesis, HCT116 does not appear to be as reliant on the tumor vasculature. Instead models such as RT112 or U87MG, with higher CD31 area densities may be more dependent on tumor angiogenesis (Fig. 4). Through the use of this high-content multiplexed imaging platform, differences between tumor models are easily profiled and databases containing information about each of the tumor models can be created. If related to differences in molecular signaling, genetics, proteomics, and drug sensitivities, a phenotypic biomarker approach may be plausible. This baseline profiling of the different tumor models not only

helps in model selection, but also reveals biological features driving tumor growth.

Phenotypic changes associated with tumor growth

In addition to knowing the baseline phenotypic profiles of tumor models, it is useful to understand the growth characteristics and kinetics of each model for improved study design. Examination of a prostate tumor model (PC3) showed that initially tumors are in a lag phase with hypoxia and apoptosis, but little proliferation. PC3 tumors at this early phase also have very few tumor vessels (Fig. 5). However, as they get larger, tumors are found to be in a log-phase of growth where proliferation is abundant, but there is little hypoxia and apoptosis (Fig. 5). This also appears to be the phase in which the ‘angiogenic switch’ occurs as the area density of blood vessels is greater during this stage. With even larger tumors a reversal of these effects are seen. The tumors become hypoxic and apoptotic with decreased area densities of tumor vessels and proliferation (Fig. 5). Having a better understanding of how tumors grow gives insight into when it is best to deliver therapeutics. For example, treating the PC3 tumors with an antiangiogenic therapy at 100 mm³ is consistent with a prevention model whereas treatments starting at 300 mm³ would be a therapeutic model. Thus, this profiling allows for a better rationale behind therapeutic interventions and provides insight into optimal study design.

Multiplexed tissue imaging to assess the effects of cancer therapeutics

The biological effects of drugs on the angiogenic, proliferative and apoptotic phenotypes of multiple models can be elucidated using this methodology. Preclinical studies have shown VEGF inhibitors reduce angiogenesis, lead to tumor vessel regression, slow tumor growth, and may improve drug delivery [22]. Using our multiplexed tissue imaging assay, we assessed the dose-dependent effects of Sorafenib, an FDA approved multikinase inhibitor targeting VEGFRs, PDGFRs, KIT, fms-like tyrosine kinase 3 (FLT3) and RAF. In the highly vascularized U87MG model, Sorafenib led to a dose-dependent reduction in CD31 and a trend for increased hypoxia (Fig. 6a,c). Consistent with previously published findings [33–35], these vascular effects were associated with decreased tumor cell proliferation and increased apoptosis (Fig. 6b,c). These results indicate that Sorafenib has multiple mechanisms of action. The antiangiogenic effect is probably from its inhibition of VEGF and PDGF signaling pathways. Inhibition of tumor cell proliferation and survival may be direct effects through inhibition of RAF, however, VEGF-selective antibodies or other multikinase inhibitors that target VEGFRs and PDGFRs, but not RAF also show antiproliferative and proapoptotic effects associated with fewer tumor blood vessels [8,36].

To further validate our imaging assays, we examined a time course effect of a cell cycle inhibitor targeting Eg5 with LY2523355. Inhibition of Eg5, a mitotic kinesin involved in early stages of mitosis and segregation of chromosomes, led to a dramatic reduction in tumor cell proliferation after five and nine days (Fig. 7). Reductions in cell proliferation were also associated with increased TUNEL area density (Fig. 7). These results are consistent with other cell cycle and Eg5 inhibitors which have shown an association between inhibition of proliferation and decreased cell

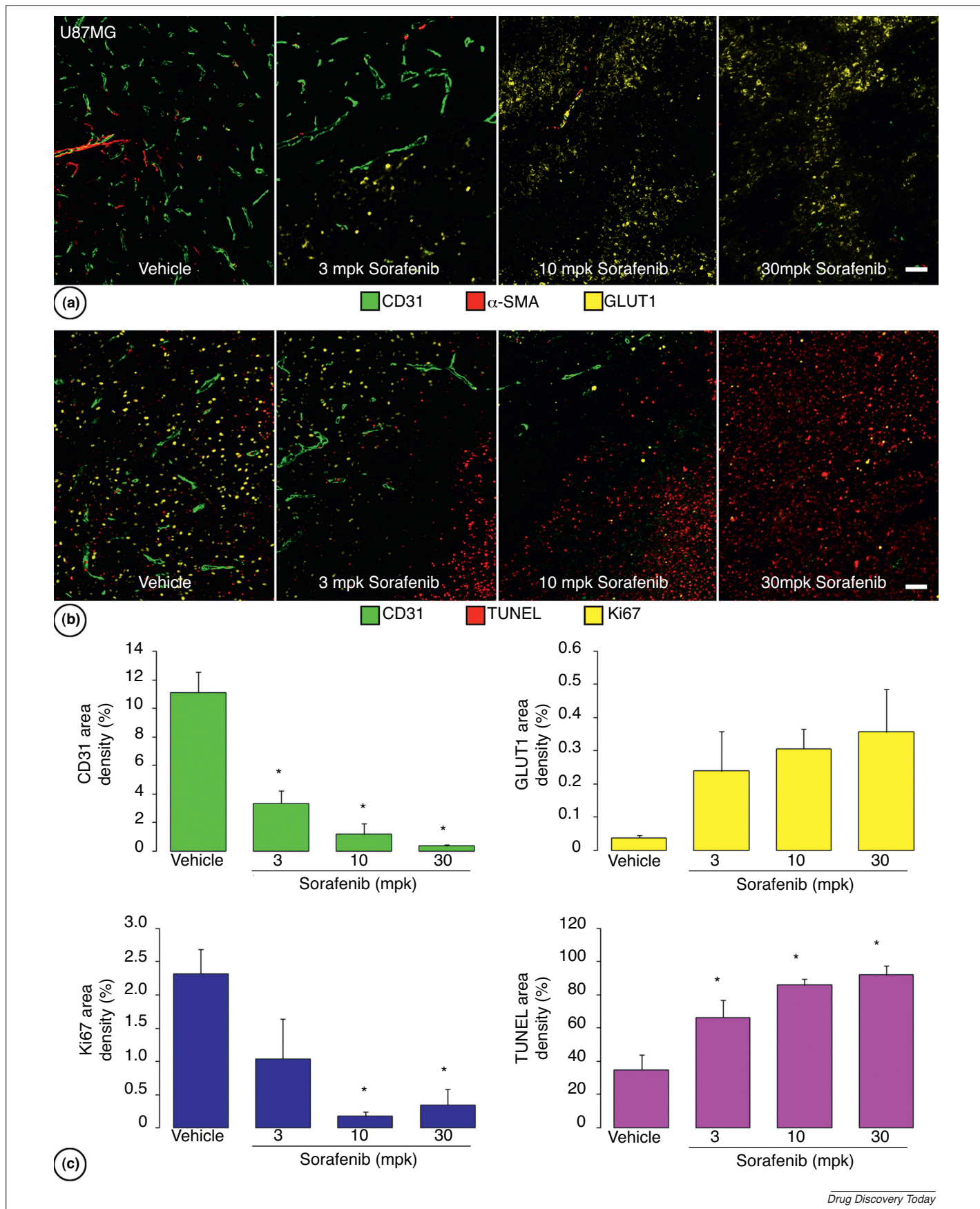
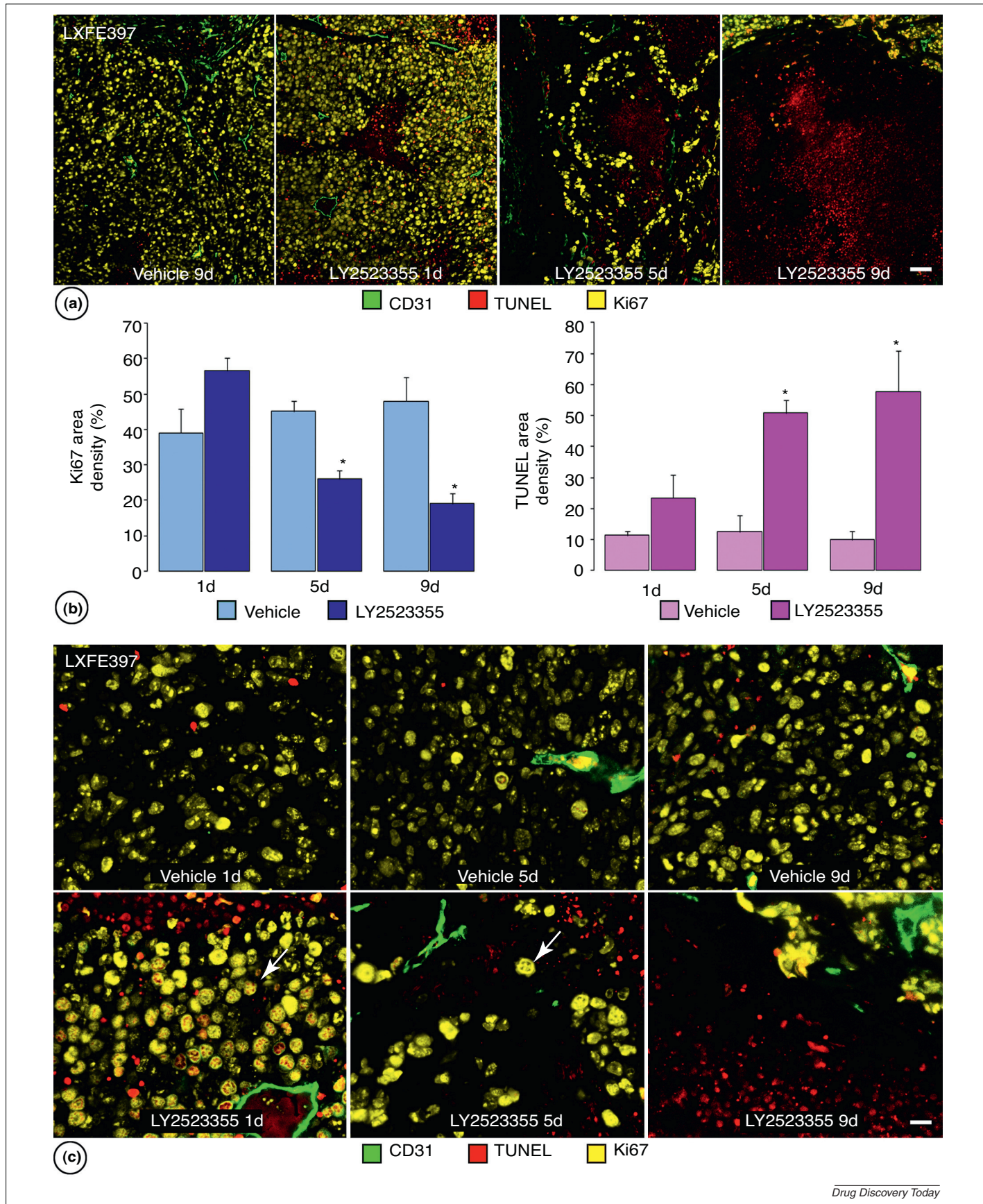


FIGURE 6

Dose-dependent effects of Sorafenib. U87MG tumors were treated for seven days with vehicle or 3, 10 or 30 mpk of Sorafenib. Micrographs show effects of Sorafenib on the angiogenesis panel (a) and tumor health panel (b). (c) Quantification of CD31, GLUT1, Ki67 and TUNEL area density after treatment. Graphs represent mean \pm SEM. N = 4–5 mice/treatment group. *P < 0.05 versus Vehicle. Scale bar is 50 μ m in (a) and (b).



Drug Discovery Today

FIGURE 7

Time course effects of a cell cycle inhibitor. **(a)** LXFE397 xenografts were treated with vehicle or an Eg5 inhibitor (LY2523355) for one, five, or nine days and stained for Ki67, TUNEL and CD31. **(b)** Area densities of Ki67 and TUNEL over the time course are shown. High magnification images show an accumulation of high Ki67 expression and monastral spindles (arrows) after treatment with LY2523355. Graphs represent mean \pm SEM. N = 3 mice/treatment group. * $P < 0.05$ versus Vehicle. Scale bar is 50 μ m in (a) and 13 μ m in (c).

survival [37–39]. Furthermore, high magnification images show the characteristic monastral spindle phenotype of prometaphase inhibition associated with Eg5 inhibition (Fig. 7c arrows). Together, these studies indicate that these high-throughput tissue imaging assays are consistent with traditional methods of analyzing the effects of drugs by IHC and are capable of studying the effects of drugs on multiple hallmarks of cancer. This can provide valuable mechanistic details and on-target validation of a variety of compound activities before performing long-term efficacy trials. In addition, the quantitative and high-throughput nature of these assays makes it feasible to support multiple drug discovery efforts in different stages of development.

Additional applications for high-throughput, multiplexed tissue imaging

Overall, these techniques are meant to be used to complement traditional IHC and pathological examination of tissues to support drug discovery. Although we focused our efforts on phenotypic characterization of tumors, multiplexed immunofluorescent tissue imaging is also amenable to target specific markers that could be used to link pharmacodynamic effects and phenotypic modulation. Similar assays could be developed to link tumor phenotypes to genetics and molecular pathways as a potential way for patient tailoring. In addition, with the growing availability of human tissue microarrays (TMAs), high-throughput methods such as this are needed to assess the phenotypic profiles and potential biomarkers of these tumors.

Although the methods described here are targeted for understanding the mechanism of action of cancer therapeutics, similar methods could be developed for other therapeutic areas.

Pathological angiogenesis has been implicated in several diseases including cardiovascular disease, macular degeneration, and several forms of autoimmune disease. Thus, the angiogenesis panel could be easily translated to the development of novel drugs across many disease states. Other IHC panels could be developed and analyzed in a similar fashion to further extend the use of the multiplexed tissue imaging analysis described here. One could examine the expression patterns and relationships of some targets of interest to either glial cells or neurons for neuroscience applications. Similar techniques could also be used to measure changes in islet size or functions for diabetes applications.

Although the angiogenesis and tumor health panels are excellent examples of assays to interrogate well validated cancer-relevant biologies, other panels are in development to understand the effects of therapeutics on other aspects of cancer therapy. These panels may further delineate project specific mechanisms of actions. For example, cell cycle regulation of a particular drug can be investigated by developing a panel to examine different phases of the cell cycle using markers such as BrDU, phosphohistone H3 and cyclin B. Additional panels to investigate effects of drugs on immune response, epithelial to mesenchymal transition, and cellular stress may also be useful for multiple drug discovery efforts. Ideally, with improvements in antibodies, it may be possible to design panels to test the effects of drugs on all the hallmarks of cancer [1,2].

Appendix A. Supplementary data

Supplementary data associated with this article can be found, in the online version, at <http://dx.doi.org/10.1016/j.drudis.2012.08.008>.

References

- Hanahan, D. and Weinberg, R.A. (2000) The hallmarks of cancer. *Cell* 100, 57–70
- Hanahan, D. and Weinberg, R.A. (2011) Hallmarks of cancer: the next generation. *Cell* 144, 646–674
- Ebos, J.M. *et al.* (2009) Accelerated metastasis after short-term treatment with a potent inhibitor of tumor angiogenesis. *Cancer Cell* 15, 232–239
- Paez-Ribes, M. *et al.* (2009) Antiangiogenic therapy elicits malignant progression of tumors to increased local invasion and distant metastasis. *Cancer Cell* 15, 220–231
- Bergers, G. *et al.* (2003) Benefits of targeting both pericytes and endothelial cells in the tumor vasculature with kinase inhibitors. *J. Clin. Invest.* 111, 1287–1295
- Bocci, G. *et al.* (2008) Antiangiogenic and anticancer effects of metronomic irinotecan chemotherapy alone and in combination with semaxinib. *Br. J. Cancer* 98, 1619–1629
- Falcon, B.L. *et al.* (2011) Increased vascular delivery and efficacy of chemotherapy after inhibition of platelet-derived growth factor-B. *Am. J. Pathol.* 178, 2920–2930
- Hashizume, H. *et al.* (2010) Complementary actions of inhibitors of angiopoietin-2 and VEGF on tumor angiogenesis and growth. *Cancer Res.* 70, 2213–2223
- Inai, T. *et al.* (2004) Inhibition of vascular endothelial growth factor (VEGF) signaling in cancer causes loss of endothelial fenestrations, regression of tumor vessels, and appearance of basement membrane ghosts. *Am. J. Pathol.* 165, 35–52
- Iwamoto, H. *et al.* (2011) Metronomic S-1 chemotherapy and vandetanib: an efficacious and nontoxic treatment for hepatocellular carcinoma. *Neoplasia* 13, 187–197
- Meier, T. *et al.* (2011) Tasisulam Sodium, an anti-tumor agent that inhibits mitotic progression and induces vascular normalization. *Mol. Cancer Ther.* 10, 2168–2178
- Noguera-Troise, I. *et al.* (2006) Blockade of Dll4 inhibits tumour growth by promoting non-productive angiogenesis. *Nature* 444, 1032–1037
- Ridgway, J. *et al.* (2006) Inhibition of Dll4 signalling inhibits tumour growth by deregulating angiogenesis. *Nature* 444, 1083–1087
- Sennino, B. *et al.* (2007) Sequential loss of tumor vessel pericytes and endothelial cells after inhibition of platelet-derived growth factor B by selective aptamer AX102. *Cancer Res.* 67, 7358–7367
- Song, S. *et al.* (2005) PDGFRbeta1 perivascular progenitor cells in tumours regulate pericyte differentiation and vascular survival. *Nat. Cell Biol.* 7, 870–879
- Winkler, F. *et al.* (2004) Kinetics of vascular normalization by VEGFR2 blockade governs brain tumor response to radiation: role of oxygenation, angiopoietin-1, and matrix metalloproteinases. *Cancer Cell* 6, 553–563
- Folkman, J. *et al.* (1966) Tumor behavior in isolated perfused organs: in vitro growth and metastases of biopsy material in rabbit thyroid and canine intestinal segment. *Ann. Surg.* 164, 491–502
- Allt, G. and Lawrenson, J.G. (2001) Pericytes: cell biology and pathology. *Cells Tissues Organs* 169, 1–11
- Hirschi, K.K. and D'Amore, P.A. (1996) Pericytes in the microvasculature. *Cardiovasc. Res.* 32, 687–698
- von Tell, D. *et al.* (2006) Pericytes and vascular stability. *Exp. Cell Res.* 312, 623–629
- Falcon, B.L. *et al.* (2009) Contrasting actions of selective inhibitors of angiopoietin-1 and angiopoietin-2 on the normalization of tumor blood vessels. *Am. J. Pathol.* 175, 2159–2170
- Baluk, P. *et al.* (2005) Cellular abnormalities of blood vessels as targets in cancer. *Curr. Opin. Genet. Dev.* 15, 102–111
- Tong, R.T. *et al.* (2004) Vascular normalization by vascular endothelial growth factor receptor 2 blockade induces a pressure gradient across the vasculature and improves drug penetration in tumors. *Cancer Res.* 64, 3731–3736
- Carroll, V.A. and Ashcroft, M. (2006) Role of hypoxia-inducible factor (HIF)-1alpha versus HIF-2alpha in the regulation of HIF target genes in response to hypoxia, insulin-like growth factor-I, or loss of von Hippel-Lindau function: implications for targeting the HIF pathway. *Cancer Res.* 66, 6264–6270
- Pennacchietti, S. *et al.* (2003) Hypoxia promotes invasive growth by transcriptional activation of the met protooncogene. *Cancer Cell* 3, 347–361
- Baumann, M.U. *et al.* (2007) Hypoxic upregulation of glucose transporters in BeWo choriocarcinoma cells is mediated by hypoxia-inducible factor-1. *Am. J. Physiol. Cell Physiol.* 293, C477–C485
- Chen, C. *et al.* (2001) Regulation of glut1 mRNA by hypoxia-inducible factor-1. Interaction between H-ras and hypoxia. *J. Biol. Chem.* 276, 9519–9525

- 28 Ouiddir, A. *et al.* (1999) Hypoxia upregulates activity and expression of the glucose transporter GLUT1 in alveolar epithelial cells. *Am. J. Respir. Cell Mol. Biol.* 21, 710–718
- 29 Hirst, D.G. *et al.* (1991) Changes in tumour morphology with alterations in oxygen availability: further evidence for oxygen as a limiting substrate. *Br. J. Cancer* 64, 54–58
- 30 Wijsman, J.A. *et al.* (2007) A practical method to determine the amount of tissue to analyse using laser scanning cytometry. *Cytometry A* 71, 501–508
- 31 Mancuso, M.R. *et al.* (2006) Rapid vascular regrowth in tumors after reversal of VEGF inhibition. *J. Clin. Invest.* 116, 2610–2621
- 32 Kuhnert, F. *et al.* (2011) Dll4–Notch signaling as a therapeutic target in tumor angiogenesis. *Vasc. Cell* 3, 20
- 33 Chang, Y.S. *et al.* (2007) Sorafenib (BAY 43-9006) inhibits tumor growth and vascularization and induces tumor apoptosis and hypoxia in RCC xenograft models. *Cancer Chemother. Pharmacol.* 59, 561–574
- 34 Kim, S. *et al.* (2007) Sorafenib inhibits the angiogenesis and growth of orthotopic anaplastic thyroid carcinoma xenografts in nude mice. *Mol. Cancer Ther.* 6, 1785–1792
- 35 Liu, L. *et al.* (2006) Sorafenib blocks the RAF/MEK/ERK pathway, inhibits tumor angiogenesis, and induces tumor cell apoptosis in hepatocellular carcinoma model PLC/PRF/5. *Cancer Res.* 66, 11851–11858
- 36 Huynh, H. *et al.* (2011) Comparing the efficacy of sunitinib with sorafenib in xenograft models of human hepatocellular carcinoma: mechanistic explanation. *Curr. Cancer Drug Targets* 11, 944–953
- 37 Esteve, M.A. *et al.* (2007) Microtubules in apoptosis induction: are they necessary? *Curr. Cancer Drug Targets* 7, 713–729
- 38 Koller, E. *et al.* (2006) Use of a chemically modified antisense oligonucleotide library to identify and validate Eg5 (kinesin-like 1) as a target for antineoplastic drug development. *Cancer Res.* 66, 2059–2066
- 39 Liu, M. *et al.* (2008) Validating the mitotic kinesin Eg5 as a therapeutic target in pancreatic cancer cells and tumor xenografts using a specific inhibitor. *Biochem. Pharmacol.* 76, 169–178